ISSN 1330-3651 (Print), ISSN 1848-6339 (Online)
https://doi.org/10.17559/TV-20240701001813
Original scientific paper

Optimal Combination of Picking Motions for Robotic Apple Harvesting Based on Experimental and Simulation Analysis

Lingxin BU, Adilet SUGIRBAY, Teng LI*

Abstract: Robotic apple harvesting requires the motion planning of a series of movements to perform the efficient picking of fruit without bruises. To optimize the picking motion of apple-harvesting robots and reduce the payload at the end of the robotic arm, this study establishes a finite element model of the branch-stem-apple system. A four-factor, three-level simulation experiment is designed to investigate the horizontal velocity, vertical velocity, bending angular velocity, and torsional angular velocity. The analysis of variance (ANOVA) and response surface methodology (RSM) analysis reveal that the four factors significantly influence the fruit detachment force. By minimizing the fruit detachment force, the simulation results of the optimized parameters suggest that horizontal pulling with bending is the optimized picking motion. The optimized parameters were tested in both simulation and field verification trials, demonstrating a high degree of consistency between the predicted detachment force and experimental measurements without causing fruit bruising during the picking process.

Keywords: apple harvesting; dynamic simulation; finite element method; fruit detachment; picking pattern; picking planning

1 INTRODUCTION

The picking patterns of harvesting robots impact the picking effect, which is attributed to the mechanical properties of the branch-stem-fruit system. This system, given its biological structure, has the ability to adapt to environmental loads, thus resisting natural loads such as wind and rain and preventing untimely fruit drop [1]. The outer layer of the apple pedicel comprises a thin peripheral layer of lamellar collenchyma, while the interior consists of thick-walled tissue (sclerenchyma), endowing it with load-resisting characteristics [2].

Cooke and Rand [3] proposed a linear dynamic theory of the fruit-stem system, simplifying it as a "double torsion spring" linear three-degree-of-freedom mechanical model. Through mathematical derivation, they predicted the natural frequencies and vibration modes of the fruit-stem system in a freely suspended state. Experimental validation was performed on apples, cherries, and grapefruits, but the impact of impulsive loads on the fruit-stem system was not considered. To study the forced vibration response characteristics of fruit tree branches, Phillips et al. [4] simplified the branch as a finite element (FE) model of a main-stem-side branch with secondary branches. They mathematically derived the vibration modes of the model with an uneven mass distribution in the length direction and different internal and external damping. While the results of computer simulations and experiments had some discrepancies, they provided valuable guidance for experimental design and theoretical adjustments. Stafford and Diener [5] studied the impacts of the apple stem motion, detachment force, and frequency on fruit detachment through mathematical modeling, providing fundamental information for mechanical apple harvesting. Yung and Fridley [6] conducted a dynamic analysis of three models, namely trunk-branch, leaf-twig, and fruit-stem models, using the finite element method (FEM). The results indicated consistency between the mathematical calculations, computer simulations, and vibration test results, demonstrating the feasibility of using the FEM to analyze the dynamic response characteristics of complex fruit tree structures. Upadhyaya et al. [7] established an FE model to describe the transient dynamic characteristics of the pedicel-branch system under branch vibration. Through mathematical analysis and experimental validation, the results suggested that when the inertia force is sufficiently large, fruit detachment can be completed within 0.1 s. The application of lateral excitation from below the branch was proven to be the most effective method for facilitating fruit detachment and reducing fruit damage [8, 9].

Additionally, some researchers have optimized apple-picking strategies by studying the motion characteristics of the hands or arms of the picker [10]. Davidson et al. [11] used sensor-equipped gloves to evaluate the picking effects of four motions, namely horizontal pulling, diagonal pulling, horizontal pulling with a twist, and diagonal pulling with a twist, on five apple varieties: Jazz, Envy, Cripps Pink, Pacific Rose, and Fuji. The optimal picking method for each variety was determined based on the stem loss rate. Li et al. [12] studied the torque-bending angle relationship and the pulling force-bending angle relationship in four picking motions using the three-finger grip of a human hand on an apple, and suggested the design of end effectors based on swinging as a picking motion. Furthermore, ADAMS software was used to construct a multibody dynamics model to study the impact of picking motions on fruit detachment. However, the model could not fully reflect details such as stress and strain [13]. Therefore, to further analyze the fruit detachment process, the combination of four picking motions was optimized in this study based on the branch-stem-fruit FE model, providing a reference for the picking motion path planning of apple-harvesting robots.

2 MATERIALS AND METHODS

2.1 Branch-Stem-Fruit Finite Element Model

The three-dimensional model of the branch-stem-fruit system was established and assembled in SolidWorks 2014. It was then imported into Abaqus 2021 software, where it was assigned material properties and meshed, as shown in Fig. 1. As the stress on the fruit core during harvesting is much less than the failure stress, the fruit model was simplified as the fruit flesh and skin [14]. The material properties of the branch, stem, detachment layer, fruit flesh, and fruit skin in the model are shown in Tab. 1. The branch and fruit flesh contained 2085 and 49726 C3D4 elements, respectively, and the fruit stem and the detachment layer were divided into 1568 C3D8 elements and 32 COH3D8 elements, respectively. The fruit skin was set as a layer of skin wrapping the fruit flesh, containing 2840 S3 (linear triangular) elements. The two ends of the branch were fixed, and the surfaces of the fruit stem and skin were defined as "hard" contact with a penalty of 0.3.

Table 1 The material parameters of the branch-stem-fruit model [15]

	Density / kg m^{-3}	Radial modulus of elasticity / MPa	Axial modulus of elasticity / MPa	Axial torsionalshear modulus / MPa	Flexural modulus / MPa	Poisson's ratio for isotropic plants	Poisson's ratio foranisotropic plants
Branch	600	29.81	181.69	10.65	337.05	0.40	0.20
Stem	300	10.34	106.42	3.70	46.90	0.40	0.11
	Density / kg m^{-3}	Initial stiffness / Nmm^{-3}	Maximum traction Force / MPa	Fractional energy release rate / kJm^{-2}			
Abscission zone	300	10000	5.01	0.71			
	Density / kg m^{-3}	Elasticity modulus / MPa	Poisson's ratio				
Cortex [16]	840	5	0.35				
Skin [16]	840	12	0.35				

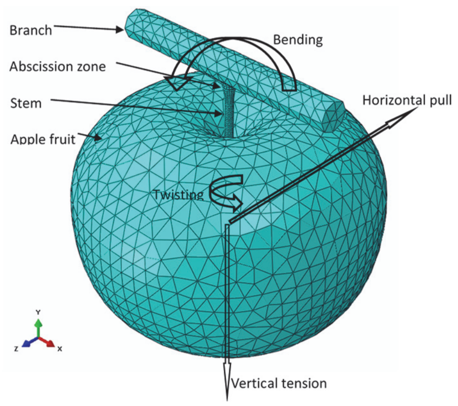

Figure 1 The FE model of the branch-stem-fruit system

2.2 Regression Analyses

Via the analysis of the influence of the picking method on fruit detachment, it was found that all four basic picking actions promoted fruit detachment. The primary factors causing fruit detachment were found to be the pulling forces, including both horizontal and vertical pulling. To further study the picking motions and provide a reference for the path planning of the robotic arm, a four-factor, three-level Box-Behnken experiment was designed using Design-Expert 8.0 software, with the four picking motions as the factors. The coding for the experiment is shown in Tab. 2.

Table 2 The factor codes of the independent variable levels

Factor	Unit	−1	0	1
Horizontal velocity (X_1)	mm s^{-1}	0	22.5	45
Vertical velocity (X_2)	mm s^{-1}	0	22.5	45
Bending angular velocity (X_3)	rads^{-1}	0	0.785	1.57
Torsional angular velocity (X_4)	rads^{-1}	0	1.57	3.14

The response surface analysis method was used to analyze the correlation between the dependent and independent variables. The dependent variable was fitted into the general form of a quadratic polynomial model, as expressed by the following equation:

$$Y = \beta_0 + \sum_{i=1}^{4} \beta_i X_i + \sum_{i=1}^{4} \beta_{ii} X_i^2 + \sum_{i=1}^{3} \sum_{j=i+1}^{4} \beta_{ij} X_i X_j \quad (1)$$

where Y represents the dependent variable, and β_0, β_i, β_{ii}, and β_{ij} denote the intercept, linear term coefficients, quadratic term coefficients, and interaction term coefficients, respectively. The desirability function ($D(x)$) is used to assess the expected level of the independent variable at selected levels, and thereby to perform multi-response optimization. The desirability function can be expressed as:

$$D(x) = (Y_1 \times Y_2 \times Y_3 \, L \, Y_n)^{1/n} \quad (2)$$

where Y_i ($I = 1, 2, \ldots, n$) represents the dependent variable, and n is the number of dependent variables.

2.3 Field Experiment Verification

Field tests were conducted from November 1 to 2, 2020, in the Huicheng Orchard in Yangling, Shaanxi Province, China. The test was carried out from 13:00 to 17:00, and the trees were ten-year-old Pink Lady apple trees. To simulate the "vertical tree wall" picking environment, wires were connected between two trees, and fruits with branches were fastened to the wire using cable ties [17]. The robotic apple harvester and test environment are shown in Fig. 2. The robotic apple harvester primarily comprises a stereo camera, a manipulator, an end-effector, and a host computer. The ZED stereovision sensor is mounted directly behind the XARM 5Lite manipulator. During the harvester's operation, the computer receives scene images transmitted by the ZED stereovision sensor and forwards them to the YOLOv4 detection algorithm for fruit target identification [18]. Once apples are identified and bounded, the left and right lenses of the ZED stereovision sensor reconstruct three dimensions by assessing the disparity of central pixels within the bounding box, enabling the spatial positioning of the fruit. Further, by transforming coordinates between the camera and the robotic arm systems, the fruit's position relative to the arm's base is determined, facilitating the calculation for kinematic inverse solutions in robotic arm path planning. The *D-H* parameters for the XARM 5Lite are presented in Tab. 3. The host computer, a Jetson TX2 equipped with a 256-core NVIDIA Pascal architecture GPU, is proficient in supporting deep learning frameworks for fruit recognition. Both the MoveIt and the vision recognition programs operate within the ROS kinetic on the Ubuntu 16.04 platform. The system architecture of the apple harvesting robot is depicted in Fig. 3, while the relationships between nodes, such as the ZED stereovision sensor, XARM 5Lite manipulator, and MoveIt, are more clearly demonstrated through the rqt-graph. As shown in Fig. 3, zed_node move_group-xarm_tral_controller path reflects the robot visual servo process. The position information of the identified fruit is transformed from the camera coordinate system to the robotic arm coordinate system. Subsequently, the inverse kinematics is resolved within Move It, and the motion planning of the robotic arm is carried out. Eventually, the robotic arm is actuated to fulfill the picking operation. The flexible end-effector features three fin-ray effect (FRE) based flexible fingers, driven by a pneumatic cylinder which actuates linkages to control grasping and releasing movements of the end-effector.

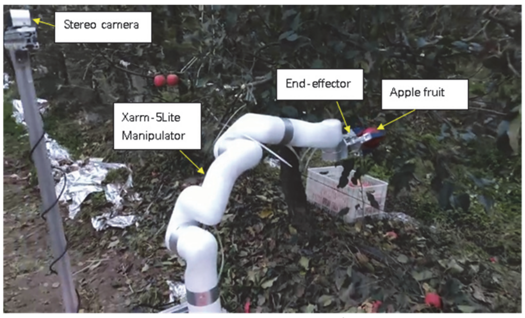

Figure 2 The experimental procedures for apple harvesting

Table 3 Standard D-H parameters of XARM 5Lite

Joint	d / mm	α / °	a / mm	Offset / °	Work scope / °
θ_1	267	−90	0	0	±360
θ_2	0	0	289.49	−79.35	−118 ~ 120
θ_3	0	0	351.16	156.60	−225 ~ 11
θ_4	0	−90	76	−77.25	±360
θ_5	97	0	0	0	−97 ~ 180

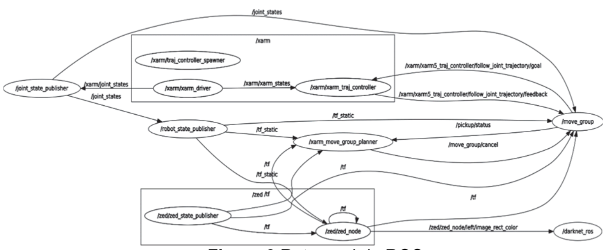

Figure 3 Rqt_graph in ROS

The base position of the arm of the apple-harvesting robot was 550 to 600 mm away from the vertical tree wall. During the fruit-picking process of the apple-harvesting robot, the joint angle q, angular velocity, angular acceleration, and joint load data were fed back by the robotic arm. The change in the fruit load during picking was estimated using Eq. (3) [19]:

$$\tau - J^T(q) h_e = D(q)\ddot{q} + C(q, \dot{q})\dot{q} + G(q) \tag{3}$$

where $D(q)$ is the inertia matrix of the robotic arm, $C(q, \dot{q})$ is the Coriolis and centripetal force coupling matrix, $G(q)$ is the gravity matrix, $J^T(q)$ is the Jacobian matrix of the robotic arm, τ is the torque matrix composed of the input loads at each joint, and he is the generalized force matrix of the external load, which is represented as $h_e = [F_x, F_y, F_z, \tau_x, \tau_y, \tau_z]$.

This equation is derived from the Newton-Euler motion equations or the Lagrangian energy method. It describes the rigid body dynamics of the robotic arm, and is also known as inverse dynamics. Thus, given the position, velocity, and acceleration of the robotic arm, the joint forces and torques can be calculated. The elements in the matrices $D(q)$, $C(q, \dot{q})$, and $G(q)$ are complex functions of the kinematic parameters of the links (θ_j, d_j, a_j, α_j) and their inertial parameters. The ten independent inertia parameters contained in each link represent the inertia of the link in a coordinate system at the origin parallel to joint coordinate system j [20]. The external load was processed and calculated using MATLAB 2018a software and its robotics toolbox 10.1 plugin. The final picking force F_{he} was calculated by Eq. (4) [21].

$$F_{he} = \sqrt{F_x^2 + F_y^2 + F_z^2} \tag{4}$$

3 RESULTS AND DISCUSSION

3.1 Regression Analyses

Fixed constraints were applied at both ends of the branch model, and the maximum detachment force during the fruit detachment process was recorded. A total of 27 sets of simulation experiments were conducted, the results of which are shown in Tab. 4.

Table 4 The experimental design comprising four independent variables at three levels, and the simulation results of the responses

	X_1	X_2	X_3	X_4	$Y(N)$
1	0	1	1	0	24.87
2	1	0	−1	0	20.75
3	0	0	−1	−1	24.52
4	−1	1	0	0	30.03
5	0	0	1	−1	20.76
6	−1	0	0	−1	27.84
7	0	0	1	1	20.69
8	0	−1	−1	0	10.01
9	0	0	0	0	22.46
10	1	−1	0	0	10.74
11	0	0	0	0	21.88
12	1	0	0	−1	19.51
13	0	0	0	0	22.91
14	0	1	−1	0	27.80
15	−1	−1	0	0	6.51
16	−1	0	0	1	27.79
17	0	−1	1	0	10.52
18	0	0	−1	1	24.39
19	0	1	0	1	26.23
20	0	1	0	−1	26.24
21	−1	0	1	0	24.62
22	1	0	0	1	19.55
23	1	1	0	0	23.52
24	0	−1	0	−1	10.69
25	0	−1	0	1	10.41
26	1	0	1	0	18.65
27	−1	0	−1	0	31.58

The simulation experiments indicated that tensile force is the main factor in fruit detachment, consistent with the findings reported by Alper and Foux [22]. Combined bending and twisting minimizes the detachment force, but it extends the picking time. The vertical tensile force contributes the most to the detachment force, suggesting that when the branch orientation approaches verticality, the fracture location may not be at the branch-pedicel junction, but at the pedicel-fruit junction, where the cross-sectional area is smaller. The regression model of the detachment force using the codes of the factors as the variables is as follows.

$$\begin{aligned} Y = {} & 22.42 - 2.97X_1 + 8.32X_2 - 1.58X_3 - 0.042X_4 - \\ & -2.69X_1X_2 + 1.21X_1X_3 + 0.022X_1X_4 - \\ & -0.86X_2X_3 + 0.068X_2X_4 + 0.015X_3X_4 + \\ & +0.67X_1^2 - 4.77X_2^2 + 0.43X_3^2 + 0.36X_4^2 \end{aligned} \tag{5}$$

The results show that X_1, X_2, X_3, X_1X_2, and X_2^2 are significant factors ($p < 0.05$). The fitted model is given by Eq. (5), with the R^2, Adj. R^2, and p-value reflecting the degree of fit of the model, and Pred. R^2 reflecting the predictive accuracy of the results. The R^2 value of 0.9598 of the fitted model demonstrates a good fit with the results of the simulation experiment. Furthermore, as shown in Tab. 6, the Pred.R^2 value (0.7701) shows good consistency with the Adj. R^2 value (0.9129).

Table 5 The ANOVA of the full-surface quadratic model responses, including the interactions of the detachment force responses

	Sum of squares	DOF	Mean square	F-value	p-value
Model	1177.26	14	84.09	20.47	< 0.0001***
X_1	105.91	1	105.91	25.79	0.0003***
X_2	830.17	1	830.17	202.13	< 0.0001***
X_3	29.89	1	29.89	7.28	0.0194*
X_4	0.021	1	0.021	5.073E−003	0.9444
X_1X_2	28.84	1	28.84	7.02	0.0212*
X_1X_3	5.90	1	5.90	1.44	0.2536
X_1X_4	2.025E−003	1	2.025E−003	4.931E−004	0.9826
X_2X_3	2.96	1	2.96	0.72	0.4126
X_2X_4	0.018	1	0.018	4.438E−003	0.9480
X_3X_4	9.000E−004	1	9.000E−004	2.191E−004	0.9884
X_1^2	2.39	1	2.39	0.58	0.4607
X_2^2	121.41	1	121.41	29.56	0.0002***
X_3^2	0.97	1	0.97	0.24	0.6349
X_4^2	0.69	1	0.69	0.17	0.6889
Residual	49.28	12	4.11		
Lack of Fit	48.75	10	4.88	18.28	0.0529
Pure Error	0.53	2	0.27		
Cor Total	1226.54	26			

Table 6 Model Summary Statistics

Std. Dev.	Mean	R^2	Adj. R^2	C.V. %	PRESS	Pred. R^2	Adeq Precision
2.03	20.94	0.9598	0.9129	9.68	282.00	0.7701	15.392

3.2 Response Surface Analysis

The ANOVA results revealed that horizontal velocity (X_1), vertical velocity (X_2), and bending angular velocity (X_3) significantly impact the fruit detachment force. Fig. 4 illustrates the responses of the detachment force to the significant factors horizontal velocity and vertical velocity when the bending angular velocity (X_3) and twisting angular velocity (X_4) are zero. The detachment force reaches its peak under the condition of a relatively low horizontal velocity and a relatively high vertical velocity. When the horizontal velocity is low, the detachment force increases significantly with the increase in vertical velocity. When the horizontal velocity is large (greater than 27 mm s^{-1}), the detachment force decreases slowly with the increase in horizontal velocity. It can be seen from the contour plot that, at any vertical velocity, the detachment force has a decreasing trend as the horizontal velocity increases; moreover, as the vertical velocity increases, the decreasing trend of the detachment force with the horizontal velocity becomes more pronounced.

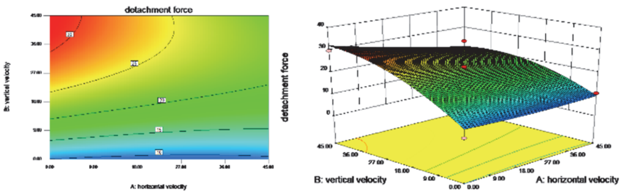

Figure 4 The contour and surface plots of the effects of the horizontal and vertical velocity on the predicted responses

Fig. 5 illustrates the responses of the detachment force to the significant factors horizontal velocity (X_1) and bending angular velocity (X_3) when the vertical velocity (X_2) and twisting angular velocity (X_4) are zero. As can be seen from Fig. 5, the detachment force tends to decrease with the increase of both the horizontal velocity and bending angular velocity.

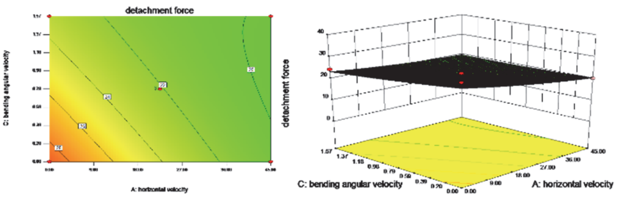

Figure 5 The contour and surface plots of the effects of the horizontal velocity and bending angular velocity on the predicted responses

Fig. 6 presents the responses of the detachment force to the significant factors X_2 (vertical velocity) and X_3 (bending angular velocity) when the horizontal velocity (X_1) and twisting angular velocity (X_4) are zero. From Fig. 6, it can be observed that the detachment force exhibits a rapid increase with the increase of the vertical velocity. At lower levels of the bending angular velocity, the variation in the detachment force with the bending angular velocity is not significant. However, at higher levels of the bending angular velocity, there is a noticeable decrease in the detachment force with the increase of the bending angular velocity. This indicates that the contribution of the bending angular velocity to the variation in the detachment force is relatively small, and higher levels of the bending angular velocity may lead to a significant reduction in the detachment force.

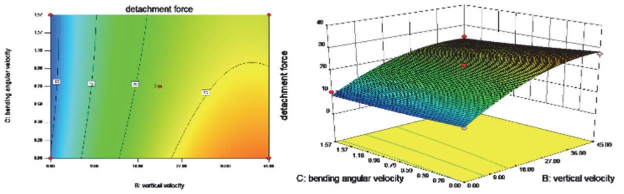

Figure 6 The contour and surface plots of the effects of the vertical velocity and bending angular velocity on the predicted responses

3.3 Parameter Optimization and Experimental Results

The ANOVA results of the simulation experiment reveal that the value of Adeq. Precision reflects the signal-to-noise ratio of the model. Its value of 15.392, which is greater than 4, indicates that the model can be used for parameter optimization. The objective of optimization is to minimize the detachment force while considering the four factors in the picking process. However, due to the structural limitations of the XARM 5Lite robotic arm, the torsional angular velocity was set to 0. The constraints and results are shown in Tab. 7 and Tab. 8, respectively.

Table 7 The specific criteria used for the optimization

Factor	Goal	Lower limit	Upper limit
Horizontal velocity (X_1) / mm s^{-1}	in range	0	45
Vertical velocity (X_2) / mm s^{-1}	in range	0	45
Bending angular velocity (X_3) / rad s^{-1}	in range	0	1.57
Torsional angular velocity (X_4) / rad s^{-1}	0	-	-
Detachment force / N	minimize	6.01	31.08

Table 8 The comparison of the results of the model optimization, simulation experiment, and field experiment

	Horizontal velocity / mm s^{-1}	Vertical velocity / mm s^{-1}	Bending angular Velocity / rads^{-1}	Twisting angular velocity / rads^{-1}	Desirability	Detachment force / N
Predicted results	6.98	0	1.57	0	0.912	8.71
Simulation experiment results	6.98	0	1.57	0	-	9.32
Field experiment results	7.00	0	1.57	0	-	10.26 ± 0.96

The optimization simulation experiments and field validation were conducted using a horizontal velocity of 6.98 mm s^{-1} and a bending angular velocity of 1.57 rad s^{-1}. In the simulation experiments, the detachment force was measured as 9.38 N, with a relative deviation of 7.69% compared to the prediction results of the model. The validation test was conducted in 50 attempts, with an average time of 13.36 ± 0.48 s per attempt, and the measured detachment force was 10.26 ± 0.96 N, with an average relative deviation of the detachment force of 9.38% compared to the results of the simulation experiment. These findings indicate the accuracy of the established FE model. Moreover, compared to previous studies, the optimized picking motion was found to be similar [13]. However, there was a significant difference between the predicted detachment force and the field experiment results, which was primarily due to the material parameters used in the model. Material parameters are influenced by factors such as the variety and picking time. Therefore, the material properties of the branches and pedicels of the tested variety (Pink Lady) were measured and used for the development of the FE model [15]. As a result, the predicted detachment force determined in this study had good consistency with the actual values.

The fruit detachment process in the FE analysis is illustrated in Fig. 7. The time it takes for the fruit to go from motion initiation to detachment is approximately 2.20 seconds. Within the initial 2.16 seconds, the pedicel straightens due to its contact with the fruit surface, gradually stretching the abscission zone and causing its stiffness to degrade. Subsequently, the cohesive elements are removed, and the fruit detachment is completed within 0.04 seconds. Therefore, under the influence of external loads, fruit detachment can occur rapidly [8].

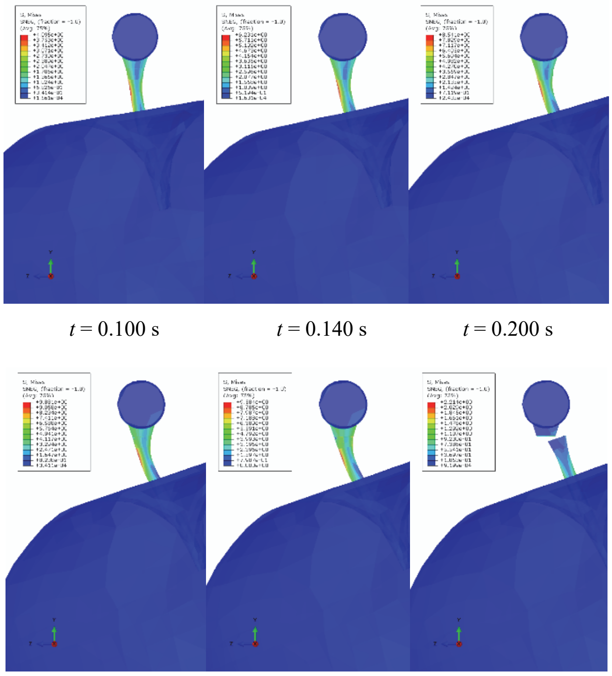

Figure 7 The fruit detachment process in the optimization simulation experiment

Fig. 8 displays the variation of the maximum von Mises stress in the fruit flesh within the contact area between the pedicel surface and the fruit skin during the fruit detachment process. At approximately 0.05 seconds, the pedicel surface comes into contact with the fruit skin. During the gradual straightening of the pedicel, the maximum von Mises stress in the fruit flesh initially rises rapidly and then stabilizes below 0.15 MPa. As the fruit continues to displace and pull the pedicel, causing a gradual decrease in the stiffness of the cohesive elements in the detachment zone, the maximum von Mises stress in the fruit flesh gradually increases. At 0.208 seconds, the maximum von Mises stress reaches 0.199 MPa, which is below the stress threshold of 0.3 MPa that could cause bruising in the fruit flesh. As the fruit detachment process progresses, under the influence of elasticity, the contact between the pedicel surface and the fruit skin is released, resulting in a rapid reduction of the maximum von Mises stress in the fruit flesh to zero. Therefore, the simulation experiment demonstrates that the fruit detachment process does not cause bruising in the fruit flesh. Correspondingly, in the field experiments, the harvested apples were kept at room temperature for 48 h without any signs of browning in the fruit flesh.

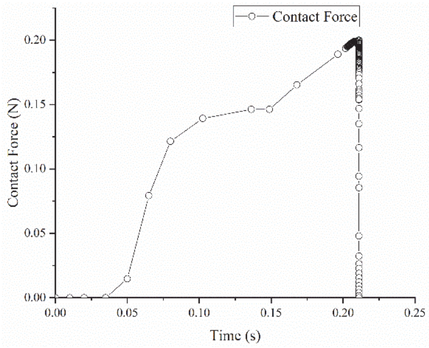

Figure 8 The change of the maximum von Mises stress of the apple cortex in the contact area with time

4 CONCLUSION

To optimize the picking motion of apple-harvesting robots and reduce the end load on the robotic arm, an FE model of the branch-stem-apple system was established in this study. Four factors (the horizontal velocity, vertical velocity, bending angular velocity, and twisting angular velocity) were designed in a four-factor, three-level simulation experiment. Variance analysis and response surface analysis were conducted to analyze the significant influences on the fruit detachment force. The ranking of the factors affecting the fruit detachment force, from most to least significant, was found to be as follows: the vertical velocity, horizontal velocity, bending angular velocity, and twisting angular velocity. By optimizing the picking motion with the objective of minimizing the fruit detachment force, the simulation experiment results indicated that horizontal pulling with bending was the optimized picking motion. Simulation experiments and field validation experiments were conducted using the optimized parameters. The results demonstrated good consistency between the predicted detachment force and the experimental measurements, and it was observed that the picking process did not cause any bruising to the fruit. By establishing the FE model and conducting comprehensive simulation and experimental analysis, this study provides valuable insights for optimizing the picking motion of apple-harvesting robots, reducing the end load on the mechanical arm, and ensuring minimal damage to the harvested fruits.

Acknowledgments

This research was supported by the Natural Science Foundation of Ningxia (No. 2023AAC03302) and North Minzu University (Grant No. 2021KYQD31).

5 REFERENCES

[1] Horbens, M., Branke, D., Gartner, R., Voigt, A., Stenger, F., & Neinhuis, C. (2015). Multi-scale simulation of plant stem reinforcement by brachysclereids: A case study in apple fruit peduncles. *Journal of Structural Biology*, *192*(1), 116-126. https://doi.org/10.1016/j.jsb.2015.08.002

[2] Lee, Y., Yoon, T. H., Lee, J., Jeon, S. Y., Lee, J. H., Lee, M. K., & Kwak, J. M. (2018). A lignin molecular brace controls precision processing of cell walls critical for surface integrity in Arabidopsis. *Cell*, *173*(6), 1468-1480, e1469. https://doi.org/10.1016/j.cell.2018.03.060

[3] Cooke, J. R. & Rand, R. H. (1969). Vibratory fruit harvesting: A linear theory of fruit-stem dynamics. *Journal of Agricultural Engineering Research*, *14*(3), 195-209. https://doi.org/10.1016/0021-8634(69)90123-1

[4] Phillips, A., Hutchinson, J., & Fridley, R. (1970). Formulation of forced vibration of tree limbs with secondary branches. *Transactions of The Asae*, *13*(1), 138-142. https://doi.org/10.13031/2013.38553

[5] Stafford, J. R. & Diener, R. G. (1973). Design criteria for minimizing predetachment fruit damage during mechanical shaking. *Transactions of The Asae*, *16*(5), 840-843. https://doi.org/10.13031/2013.37640

[6] Yung, C. & Fridley, R. B. (1975). Simulation of vibration of whole tree systems using finite elements. *Transactions of The Asae*, *18*(3), 475-481. https://doi.org/10.13031/2013.36613

[7] Upadhyaya, S. K., Cooke, J. R., & Rand, R. H. (1981). Limb impact harvesting, part I: finite element analysis. *Transactions of The Asae*, *24*(4), 856-863. https://doi.org/10.13031/2013.34352

[8] Upadhyaya, S. K., Cooke, J. R., Pellerin, R. A., & Throop, J. A. (1981). Limb impact harvesting, part II: experimental approach. *Transactions of The Asae*, *24*(4), 864-867. https://doi.org/10.13031/2013.34353

[9] Upadhyaya, S. K., & Cooke, J. R. (1981). Limb impact harvesting, part III: model studies. *Transactions of The Asae*, *24*(4), 868-878. https://doi.org/10.13031/2013.34354

[10] Zhang, Z., Zhang, Z., Wang, X., Liu, H., Wang, Y., & Wang, W. (2019). Multi-purpose apple harvest platform economic evaluation modeling and software development. *International Journal of Agricultural and Biological Engineering*, *12*(1), 74-83. https://doi.org/10.25165/j.ijabe.20191201.4360

[11] Davidson, J., Silwal, A., Karkee, M., Mo, C., & Zhang, Q. (2016). Hand-picking dynamic analysis for undersensed robotic apple harvesting. *Transactions of the ASABE*, *59*(4), 745-758. https://doi.org/10.13031/trans.59.11669

[12] Li, J., Karkee, M., Zhang, Q., Xiao, K., & Feng, T. (2016). Characterizing apple picking patterns for robotic harvesting. *Computers and Electronics in Agriculture*, *127*, 633-640. https://doi.org/10.1016/j.compag.2016.07.024

[13] Bu, L., Hu, G., Chen, C., Sugirbay, A., & Chen, J. (2020). Experimental and simulation analysis of optimum picking patterns for robotic apple harvesting. *Scientia Horticulturae*, *261*, 108937. https://doi.org/10.1016/j.scienta.2019.108937

[14] Ji, W., Qian, Z., Xu, B., Tang, W., Li, J., & Zhao, D. (2017). Grasping damage analysis of apple by end-effector in harvesting robot. *Journal of Food Process Engineering*, *40*(6), e12589. https://doi.org/10.1111/jfpe.12589

[15] Bu, L., Chen, C., Hu, G., Zhou, J., Sugirbay, A., & Chen, J. (2021). Investigating the dynamic behavior of an apple branch-stem-fruit model using experimental and simulation analysis. *Computers and Electronics in Agriculture*, *186*, 106224. https://doi.org/10.1016/j.compag.2021.106224

[16] Ahmadi, E., Barikloo, H., & Kashfi, M. (2016). Viscoelastic finite element analysis of the dynamic behavior of apple under impact loading with regard to its different layers. *Computers and Electronics in Agriculture*, *121*, 1-11. https://doi.org/10.1016/j.compag.2015.11.017

[17] Hu, G., Zhou, J., Chen, Q., Luo, T., Li, P., Chen, Y., Zhang, S., &Chen, J. (2024). Effects of different picking patterns and sequences on the vibration of apples on the same branch. *Biosystems Engineering*, *237*, 26-37. https://10.1016/j.biosystemseng.2023.11.010

[18] Galić, D., Stojanović, Z., & Čajić, E. (2024). Application of neural networks and machine learning in image recognition. *Tehnički Vjesnik*, *31*(1), 316-323. https://doi.org/10.17559/TV-20230621000751

[19] Siciliano, B., Sciavicco, L., Villani, L., & Oriolo, G. (2010). *Robotics: modelling, planning and control*: Springer Science & Business Media.

[20] Corke, P. (2013). *Robotics, Vision and Control: Fundamental Algorithms in MATLAB*: Springer Publishing Company, Incorporated.

[21] Burghardt, A., Kurc, K., & Szybicki, D. (2020). Automatic detection of industrial robot tool damage based on force measurement. *Tehnički Vjesnik*, *27*(5), 1385-1393. https://doi.org/10.17559/TV-20181110163252

[22] Alper, Y. & Foux, A. (1976). Strength properties of orange fruit-stem joints. *Transactions of The Asae*, *19*(3), 412-416. https://doi.org/10.13031/2013.36040

Contact information:

Lingxin BU
College of Mechatronic Engineering,
North Minzu University,
Yinchuan, Ningxia, 750021, China
E-mail: 2021023@nmu.edu.cn

Adilet SUGIRBAY
Polytechnical Institute,
West Kazakhstan Agricultural and Technical University Named after Zhangir Khan, Uralsk 090009, Kazakhstan
E-mail: adilet_s_93@mail.ru

Teng LI
(Corresponding author)
School of Electrical and Electronic Engineering,
Wuhan Polytechnic University,
Wuhan 430023, China
E-mail: liteng013@whpu.edu.cn